IOP Publishing Smart Materials and Structures
Smart Mater. Struct. 27 (2018) 115003 (13pp) https://doi.org/10.1088/1361-665X/aae0b0

Development of elasto-magnetic (EM) sensor for monitoring cable tension using an innovative ratio measurement method

Liang Ren[1], Chengzhu Xiu[1,2], Hongnan Li[1,3], Ye Lu[2], Jiajian Wang[1] and Xuejia Yao[1]

[1] State Key Laboratory of Coastal and Offshore Engineering, Dalian University of Technology, Dalian, 116023, People's Republic of China
[2] Department of Civil Engineering, Monash University, Clayton, VIC 3800, Australia
[3] School of Civil Engineering, Shenyang Jianzhu University, Shenyang, 110168, People's Republic of China

E-mail: xiucz@mail.dlut.edu.cn

Received 27 June 2018, revised 9 September 2018
Accepted for publication 12 September 2018
Published 25 September 2018

Abstract

The magnetic permeability changes of ferromagnetic materials under elastic stress offer the potential to measure tension based on the inverse magnetostrictive effect. The elasto-magnetic (EM) sensor is the most promising technology for monitoring tension in steel structures. Nevertheless, difference in the device channel or variation of the external wire resistance results in an inaccurate induced voltage variation of the EM sensor in tension measurement. In this paper, the EM sensor for monitoring cable tension using an innovative ratio measurement method was presented. An inductor-resistor model of the excitation system and a transformer model of the sensor system were established to obtain the explicit relationship between the ratio result and the external tension. The experimental results show that the ratio of the integral value of the induced voltage to the excitation current variation is proportional to the external tension, a finding that is consistent with the theoretical derivation. In addition, the simulation analysis and experiment result demonstrate that the ratio measurement method improves sensor performance with the comparison of the traditional induced voltage method. Finally, the EM sensor was applied in the Zhengzhou Olympic Stadium of China. The monitoring results show that the proposed ratio measurement method could accurately measure cable tension.

Keywords: tension measurement, elasto-magnetic (EM) sensor, steel cable, induced voltage method, ratio measurement method

(Some figures may appear in colour only in the online journal)

1. Introduction

Nowadays, more and more newly built or existing critical civil infrastructures are equipped with recently emerged structural health monitoring (SHM) systems because unpredicted structural failure can cause economic, catastrophic, and human life loss [1, 2]. SHM is a new concept to the field of civil engineering and is intended to monitor structural behavior in real-time, to evaluate structural performance under various loads, and to identify structural damage or deterioration [3, 4]. More specifically, it is imperative to measure cable tension using SHM technologies during the service life of steel structures. Damage in steel cables can induce collapse of structural components and result in the failure of entire infrastructures [5–7]. However, it is a challenging task to determine the accurate tension value in steel cables under external loads and varying circumstances during structural service life [8].

Currently, cable tension can be measured directly by the load measurement sensors or estimated from certain parameters related to the responses of the cable, such as strain, acceleration, or magnetic permeability. The former can be

defined as the direct method, whereas the latter is known as the indirect method [9]. Cho *et al* [10] proposed the direct method with a load cell or pressure meter installed at one end of a cable. Although the direct method is usually accurate and straightforward, it is unsuitable after the construction. Among the responses to indirect methods, acceleration is the most widely used parameter in practice. Li *et al* [11], Heo *et al* [12], Bao *et al* [13], and Wu *et al* [14] presented the vibration frequency method, in which an acceleration signal was acquired to estimate cable tension, which was based on the relation between the natural frequency of the cable vibrations and the tension force in the cable. However, uncertainties in some parameters, such as mass, length, and cross-sectional area, can generate significant errors in the actual force value [15, 16]. Moreover, the measurement accuracy of the vibration frequency method is affected by many factors, such as the bending rigidity and boundary condition of the cable, the installation of damping devices, and the effect of cable poly ethylene (PE) bushing [17]. On the other hand, it is infeasible to measure the actual cable tension using strain gauges because cables contain tens or hundreds of twisted wires or strands sheathed in a plastic protective cover or a duct filled by cement grout or grease [18].

In contrast, an EM sensor based on the magneto-elastic effect in ferromagnetic materials as a novel non-destructive method for measuring cable tension in pre-stressed structures and bridge cables was introduced by Singh *et al* [19] and Sumitro *et al* [20]. This technology enables users to overcome some of the problems associated with conventional methods. Hence, it is a promising method for tension monitoring of steel cables due to its corrosion resistance, strong overloading capacity, long life-span, and accurate tension measurement, features that are not easily influenced by the vibration and the PE layer of steel cables [21]. The EM sensor usually consists of a primary excitation coil providing variable flux to the measured steel specimen and a secondary induction coil wound inside the excitation coil to obtain the induced voltage originated from the excitation magnetic field. According to Faraday's law of electromagnetic induction, the induced voltage acquired by the secondary coil is directly proportional to the change rate of the applied magnetic flux [22]. In recent years, to install EM sensors easily for tension measurement, Ricken *et al* [23–25] and Roy *et al* [26] had developed EM sensors with C-shaped or E-shaped structures for straightforward installation in practical engineering, respectively. Tang *et al* [27] studied a steel strand tension sensor with difference single bypass excitation structure. In these applications, the steel cables act as a part of the magnetic circuit of the EM sensor, and tension variation is therefore detected by the secondary coil. The flexible printed coil as a replacement for the traditional hard coil was also invented by Tse *et al* [28] to facilitate the installation and disassembly of the sensor. However, the existing EM sensor usually uses the induced voltage to evaluate the cable tension. The excitation current can be changed due to difference in the device channel or variation of the external wire resistance, which will affect the tension measurement of the EM sensor and reduce the sensor sensitivity.

In this paper, an EM sensor for monitoring cable tension using an innovative ratio measurement method was presented. The inductor-resistor (LR) model of the excitation system was proposed to demonstrate that a difference in the device channel or a variation of the external wire resistance has an effect on the excitation current, resulting in an inaccurate induced voltage variation in the secondary coil. Furthermore, the transformer theoretical model of the sensor system was established to obtain the explicit relationship between the ratio result and the external tension. The finite element simulations and experimental studies are conducted to investigate the sensor performance with induced voltage method and ratio measurement method. The layout of this paper is as follows. Section 2 elaborates the theoretical derivations of the LR model of the excitation system and the transformer model of the sensor system. In section 3, the finite element analysis of the sensor model is introduced. Then, an experiment in factory calibration is carried out and measurement results using the induced voltage method and the ratio measurement method are discussed in section 4. Section 5 shows the tension results in the Zhengzhou Olympic Stadium of China as a case study. Finally, the conclusions and future works are detailed in section 6.

2. Theoretical model

2.1. EM sensor principle

The EM sensor consists principally of a primary coil and a secondary coil wound on the test specimen, which function cooperatively to formalize the magneto-elastic characterization of the material. The ferromagnetic material has a unique relationship (known as a magnetization curve) between the applied magnetic field strength and the resulting magnetic flux density. The magnetic permeability, which is an important parameter of magnetic material, can be expressed as:

$$\mu = B/H, \tag{1}$$

where B is the magnetic flux density, H is the magnetic field strength, and μ is the magnetic permeability of magnetic material.

With an alternating or a pulse current signal passing through the primary coil, the associated magnetic field is applied in the primary coil and the resulting magnetic flux density in the test specimen produces an electromotive force in the secondary coil due to electromagnetic induction. According to Faraday's law, the electromotive force induced in the secondary coil is proportional to the time change in the magnetic flux inside the coil, given by [29]:

$$\varepsilon_{\text{out}} = -N\frac{d\phi}{dt} = -N\left[\mu_0(A_s - A_t)\frac{dH(t)}{dt} + A_t\frac{dB(t)}{dt}\right], \tag{2}$$

where ε_{out} is the electromotive force, N is the the number of coil turns, ϕ is the magnetic induction, μ_0 is the vacuum permeability, and A_s and A_t stand for cross-sectional areas of the secondary coil and test specimen, respectively.

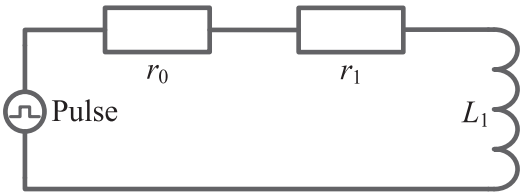

Figure 1. LR model of excitation system.

Under a constant magnetic field in the excitation coil, the integral value of the induced voltage across the secondary coil with and without the test specimen can be expressed as follows [30]:

$$V_c = -\int_{t_1}^{t_2} \varepsilon_{\text{out}} dt = N[\mu_0(A_s - A_t)\Delta H + A_t \Delta B], \quad (3)$$

$$V_0 = NA_s\mu_0\Delta H, \quad (4)$$

where V_c and V_0 represent the integral value of the induced voltage across the secondary coil with and without the test specimen, respectively. Solving equations (3) and (4), the magnetic permeability is derived by:

$$\mu_r = 1 + \frac{A_s}{A_t}\left(\frac{V_c}{V_0} - 1\right). \quad (5)$$

Since A_t, A_s and V_0 are constants, V_c is the sole variable of μ_r. Therefore, equation (5) shows the existence of a linear relationship between the integral value of the induced voltage across the secondary coil and the magnetic permeability.

2.2. LR model of excitation system

A pulse signal with a string of frequency components is selected as the excitation signal and applied to the primary coil. The capacitance from adjacent coil rings or the coaxial cable is negligible due to the pulse signal in the low-frequency range. Therefore, the excitation system can be modeled through the LR circuit, as shown in figure 1.

The first-order linear differential equation of the excitation system can be given by:

$$L_1\frac{di_1(t)}{dt} + Ri_1(t) = U_s(t), \quad (6)$$

where L_1 is the inductance of the primary coil, R is the sum of the external wire resistance r_0 and the coil internal resistance r_1, i_1 and U_s are the excitation current and voltage, respectively. Solving equation (6), the current passing through the excitation coil i_1, the inductor voltage U_i and the voltage across the primary coil U_c can be expressed as follows:

$$i_1(t) = \frac{A}{R} - \frac{A}{R}e^{-\frac{R}{L_1}t}, \quad (7)$$

$$U_i(t) = Ae^{-\frac{R}{L_1}t}, \quad (8)$$

$$U_c(t) = \frac{Ar_1}{R} + \left(1 - \frac{r_1}{R}\right)Ae^{-\frac{R}{L_1}t}, \quad (9)$$

where A is the magnitude of the excitation voltage. When a pulse excitation voltage passes through the sensor coil, the excitation current changes on rising or falling edge of the excitation voltage due to the inductance of the coil, which yields the coil voltage and induced voltage change accordingly, as shown in figure 2.

2.3. Transformer model of sensor system

The transformer model of the sensor system in figure 3 presents the work principle of the EM sensor. The magnetic flux density is produced when a changed signal flows through the excitation coil. Based on Faraday's law, the induced signal across the secondary coil is observed, which is opposite to the excitation signal.

In accordance with Kirchhoff's voltage law and Faraday's electromagnetic induction law, the following equations can be expressed:

$$U_1 = i_1r_1 + N_1\frac{d\phi_1}{dt}, \quad (10)$$

$$U_2 = -N_2\frac{d\phi_2}{dt}, \quad (11)$$

$$\phi_1 = \phi_2 + \phi_3, \quad (12)$$

where U_1 and U_2 are the excitation voltage and induced voltage, N_1 and N_2 are the turns of the excitation coil and induced coil, ϕ_1 and ϕ_2 are the magnetic inductions of excitation coil and induced coil, ϕ_3 is the leakage magnetic induction, which is ignored due to the the magnetic permeability of the test specimen higher than that of the non-magnetic skeleton.

Solving equations (7)–(12), the ratio of the integral value of the induced voltage to the excitation current variation can be derived by:

$$RM = \left|\frac{V_{\text{out}}}{\Delta i(t)}\right| = \frac{k_1N_1N_2A_t\mu_0}{l}u_r, \quad (13)$$

where V_{out} represents the integral value of the induced voltage U_2, $\Delta i(t)$ is the excitation current variation, l is the length of primary coil, A_t stands for cross-sectional area of the test specimen, and k_1 is the coupling coefficient, respectively.

The ratio of the integral value of the induced voltage to the excitation current variation is defined as the parameter proportional to the relative permeability in cable tension measurement. However, the excitation current may be changed due to difference in the device channel or variation of the external wire resistance, which would affect the tension measurement results of a traditional EM sensor using the induced voltage method. Hence, the ratio measurement method is proposed in this study and the effect of the excitation current on the measured result would be eliminated, which is beneficial for improving the sensor performance.

3. Finite element analysis

3.1. Sensor structure

A 2D axis-symmetric model of EM sensor was established using finite element analysis software ANSYS 17.0 [31]. Two solenoid coils (primary and secondary coils), are wound on the steel cable as shown in figure 4. When a pulse current

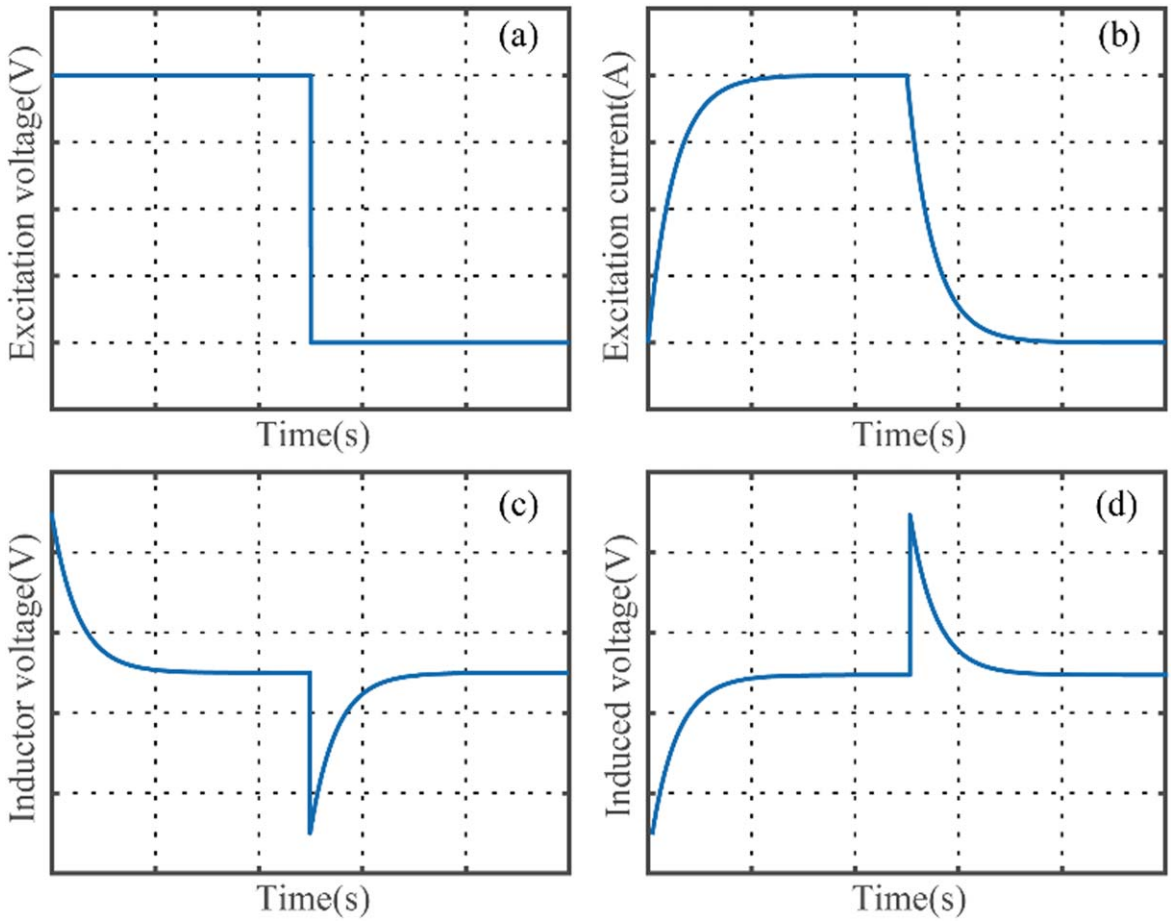

Figure 2. Sensor input and output signal waveforms ((a) excitation voltage signal (b) excitation current signal (c) inductor voltage signal (d) induced voltage signal).

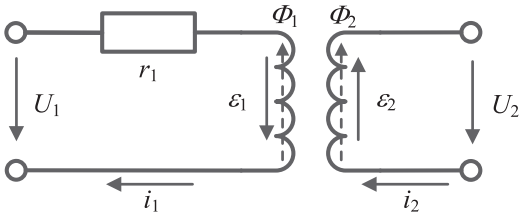

Figure 3. Transformer model of the sensor system.

signal is applied to the primary coil, the exciting magnetic field is produced. According to Faraday's law, the induced signal is produced across the secondary coil, which is opposite to the excitation signal [32–34]. The EM sensor structure consists of the two coils, silicone pad, steel cover, and connect fitting attached to the non-magnetic skeleton. The steel cover protects the sensor structure and enhances the sensor stability to make it safe and reliable over the long term. It also enhances the shielding effectiveness of the sensor and reduces the impact of external electrical devices.

3.2. Magnetic induction distribution

The physical field of finite element analysis was selected as the magnetic field under a pulse excitation and then solved using the transient solver. The magnetic field lines are set parallel to the external boundaries of the transformer model. The direction of the sensor's axis is defined as the *Y*-axis, and the *XOZ* plane overlaps with the middle of the sensor. The normalized magnetic induction of excitation coil is depicted in figure 5.

It can be seen from the simulation results shown in figure 5 that the magnetic induction mainly passes through the test specimen because the magnetic permeability of the test specimen is higher than that of the non-magnetic skeleton. Therefore, the leakage magnetic induction can be ignored, which verifies the rationality of the theoretical derivation. The magnetic induction nearby the *X*-axis of 50 mm is slightly higher than that in other position of the test specimen. This is considered a reasonable result because the secondary coil is installed in this position and it would have an effect on the magnetic induction distribution.

3.3. Variation of the external wire resistance

The external wire resistance variates from 0% to 10% with an increment of 2%. Based on the theoretical derivation of equations (6)–(9), the excitation current and induced voltage will be changed accordingly as shown in figure 6.

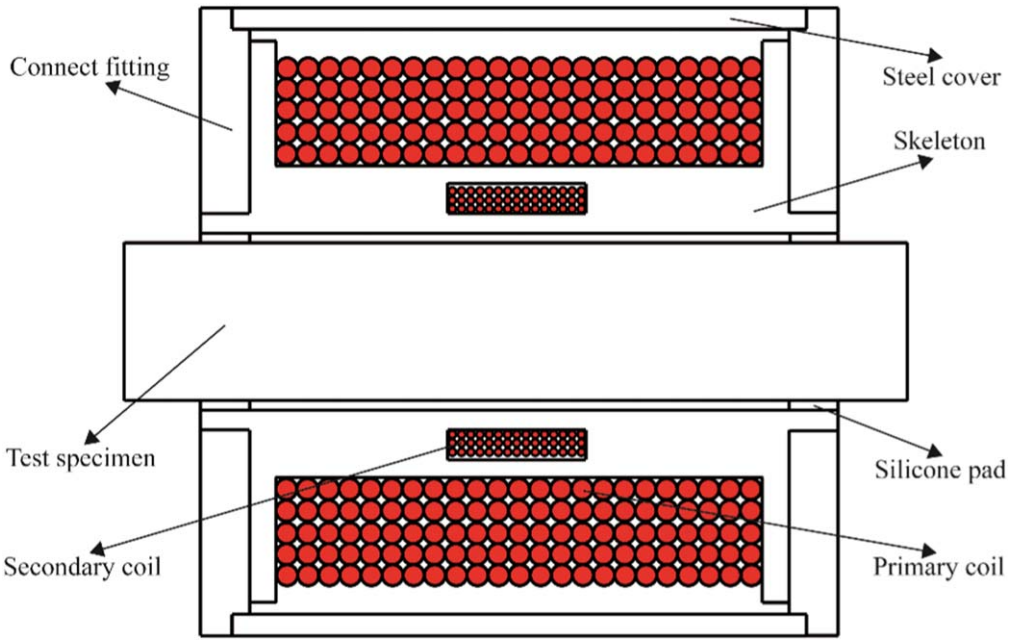

Figure 4. Schematic diagram of sensor structure.

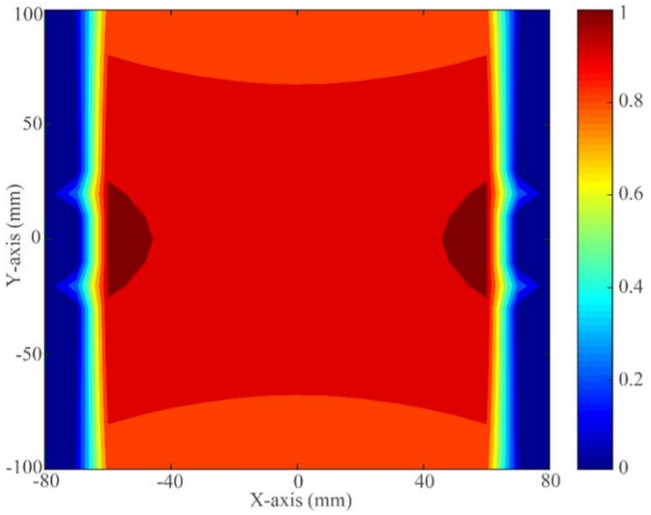

Figure 5. Normalized magnetic induction of excitation coil.

The simulation results in figure 6 suggest that the excitation current and the induced voltage decrease with increasing the variation of the external wire resistance, which would affect the tension measurement results of a traditional EM sensor using the induced voltage method. Therefore, the ratio measurement is proposed and the effect of variation of the external wire resistance would be eliminated. The simulation results in two measurement methods are shown in figure 7. It can be seen from figure 7 that when the external wire resistance has the variation of 10%, the sensor output results will be changed with 2.8% using the traditional induced voltage method and are almost unchanged using the ratio measurement method.

4. Experimental setup

4.1. Sensor system

The cable tension monitoring is achieved by the sensor system as shown in figure 8, which mainly includes three parts: the EM sensor, the signal acquisition instrument, and LabVIEW monitoring module. The EM sensor is utilized to measure the magnetic field variation caused by the action of tension on the test specimen. The developed signal acquisition instrument not only generates an appropriate excitation signal passing through the primary coil for magnetizing the test specimen, but also picks up the induced signal across the secondary coil. After the sensor signals pass through the proper data processing device and analog-to-digital (A/D) converter, the result can be viewed synchronously on the computer by the LabVIEW monitoring module.

4.2. Comparison of two measurement methods

The sensor signal was excited and collected through a 16-channel data acquisition system consisting of the excitation model, gain amplifier, low pass filter and integral circuit. Some slight difference existed among the 16 channels of the acquisition instrument due to deviation of the electronic components. The induced voltage results and ratio results are measured by three times at each channel. The statistics results of six devices calculated by the averaged results in two measurement methods are listed in table 1.

Table 1 demonstrates that both the standard deviation and coefficient of variation of the ratio measurement results are smaller than those of the induced voltage results. The coefficient of variation, not the standard deviation, was selected as

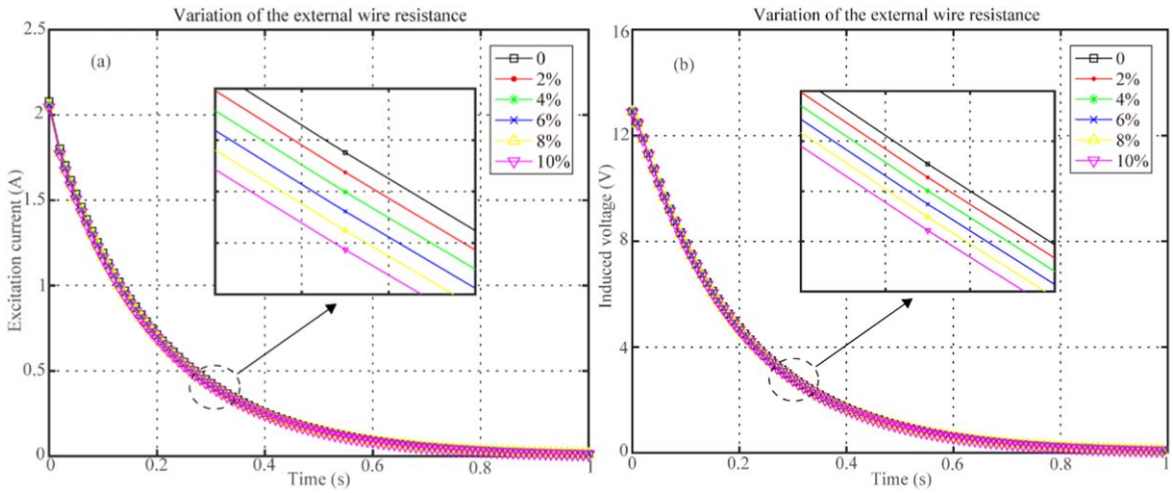

Figure 6. Simulation results obtained by changing the external wire resistance. (a) Excitation current results and (b) induced voltage results.

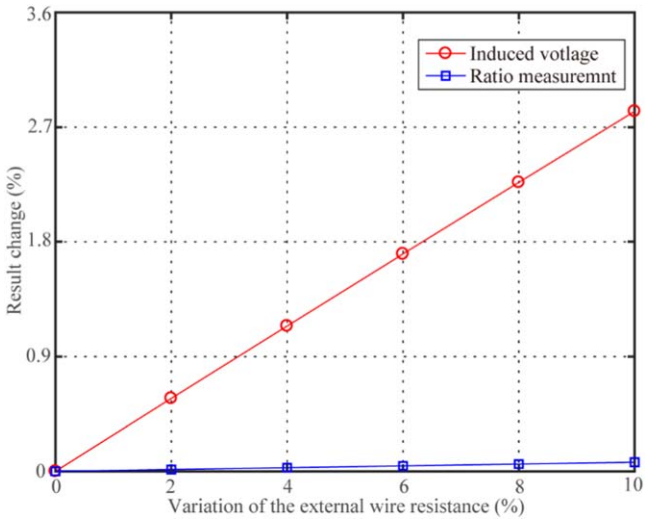

Figure 7. Comparison of sensor output results in two measurement methods by variating the external wire resistance.

the comparison parameter due to the different dimensions of the induced voltage result (mV) and the ratio measurement result (mV mA^{-1}). The coefficients of variation in two measurement methods are less than 2%, which means that the difference among the 16 channels is small. Moreover, the coefficient of variation of the proposed ratio measurement method is smaller than that of the traditional induced voltage method as shown in figure 9, indicating the improvement in the sensor performance with the proposed ratio measurement method.

4.3. Factory calibration

The Zhengzhou Olympic Stadium with a 60 000 seat capacity is the largest stadium in Hebei Province of China, consisting mainly of the suspended grid structure shown in figure 10. The north–south and east–west dimensions of the stadium are approximately 291.5 m and 311.6 m. The total building height and area are 54.39 m and 138 500 m^2, respectively. The Zhengzhou Olympic Stadium is composed of 42 radial and 32 circular cables, that are comprised the main bearing structure. Detailed specifications for the steel cables are listed in table 2. Since this stadium is exposed to a severe natural environment, monitoring its real-time health status during its service life is of significant importance and necessity.

To utilize the EM sensors for tension measurement in real-world practice, the EM sensors were attached to the cables and the factory calibration tests were conducted in the cable factory Jian Yi Jia Co. Limited (Shenzhen). Compared with the force transducer, the EM sensor has the advantage of larger measurement range, longer life and does not require physical contact with the steel cable itself. As shown in figure 11, each cable was connected in turn to a hydraulic prestressing jack applying the necessary tension loads indicated by a load cell. The radial and circular cables were loaded up to a tension of 3000 kN in steps of 300 kN and 4500 kN with an increment of 500 kN, respectively. The experiment result of the sensor is shown in figure 12, which is in accordance with the theory and simulation results.

After each load step, the sensor response was acquired by the system and then fitted with the applied cable tension. Three repetitive experiments were completed to reduce the test error and the averaged results were analyzed. As shown in figure 13, the three repeated experimental results of two measurement methods were almost identical. Besides, it was apparent that with the increase in tension, the experimental results of both the integral value of the induced voltage and the ratio measurement decreased.

To compare the sensor performance of these two measurement methods, the relative sensitivity is proposed as

$$S = \left| \frac{Y(T) - Y(T_0)}{Y(T_0)(X(T) - X(T_0))} \right|, \tag{14}$$

where S is the relative sensitivity, $X(T)$ and $X(T_0)$ are the tensions in the initial condition and at a certain stage, respectively, and $Y(T)$ and $X(T_0)$ are the corresponding outputs of the sensor. Under the same experimental conditions, the relative sensitivity variations of the two measurement methods were compared as shown in figure 14.

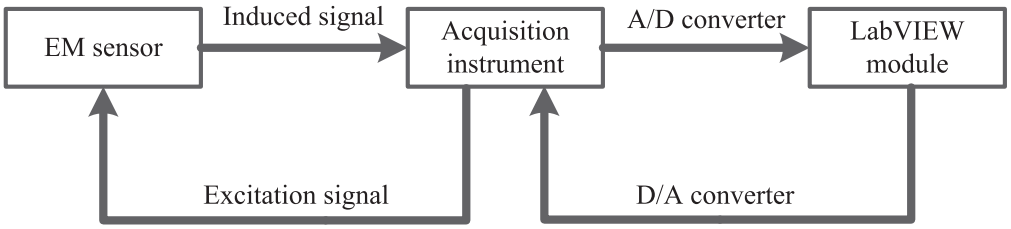

Figure 8. Schematic illustration of the sensor system.

Table 1. Statistics results of six devices in two measurement methods.

Devices	Measurement methods	Standard deviation	Coefficient of variation (%)
1st	Induced voltage	1.34 (mV)	0.822
	Ratio measurement	0.005 99 (mV mA^{-1})	0.498
2nd	Induced voltage	2.83 (mV)	1.772
	Ratio measurement	0.007 67 (mV mA^{-1})	0.644
3rd	Induced voltage	0.756 (mV)	0.487
	Ratio measurement	0.003 44 (mV mA^{-1})	0.293
4th	Induced voltage	1.80 (mV)	1.150
	Ratio measurement	0.009 25 (mV mA^{-1})	0.771
5th	Induced voltage	0.893 (mV)	0.568
	Ratio measurement	0.523 (mV mA^{-1})	0.442
6th	Induced voltage	1.43 (mV)	0.892
	Ratio measurement	0.007 14 (mV mA^{-1})	0.595

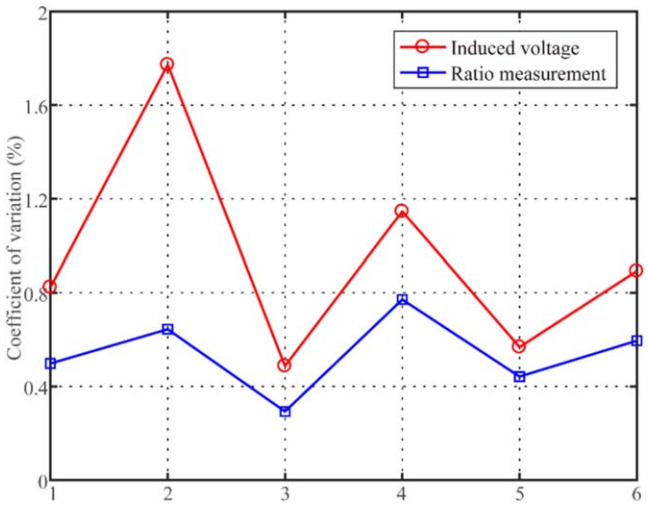

Figure 9. Comparison of coefficients of variation in two measurement methods.

Figure 10. The Zhengzhou Olympic Stadium.

It can be seen from the figure 14 that the good linearity between the ratio measurement results and the tension loads indicates that the ratio measurement method can be effectively used to measure cable tension. Compared with the induced voltage method, the ratio measurement method has a higher relative sensitivity as listed in table 3. As shown in figure 14 and table 3, the fitting curves for the radial cable using the ratio measurement method and the induced voltage method in the loading process between cable tension force and measurement parameters are shown as:

$$RM = 0.30\%F - 0.81, \tag{15}$$

$$IV = 0.27\%F - 0.65. \tag{16}$$

In the unloading process, the fitting curves can be expressed as:

$$RM = 0.31\%F - 0.91, \tag{17}$$

$$IV = 0.28\%F - 0.83. \tag{18}$$

In the factory calibration of the radial cable, the relative sensitivity of the sensor is improved by 11.1% from 0.27%/kN to 0.3%/kN and by 10.7% from 0.28%/kN to 0.31%/kN during the loading and unloading processes, respectively. Similar conclusions are evident for the circular cable.

Figure 11. The experimental setup for factory calibration.

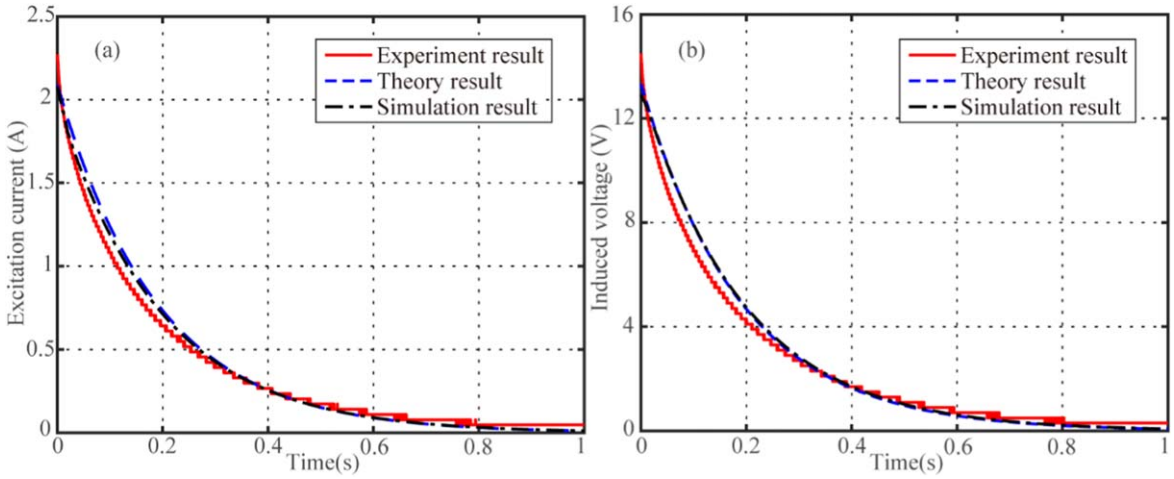

Figure 12. (a) Excitation current signal and (b) induced voltage signal of the sensor.

Table 2. Specifications of the steel cables.

Properties	Cables			
	Radial cables			Circular cables
Cable-type	High vanadium cable	High vanadium cable	High vanadium cable	Sealing cable
Diameter (mm)	116	119	140	130
Elastic modulus (kN m^{-2})	1.6	1.6	1.6	1.6
Nominal area (mm^2)	7940	8320	11 470	11 469
Minimum breaking force (kN)	11 670	12 230	16 470	16 200

5. Engineering application

5.1. EM sensor layout

The large open spoke type suspended grid structure was adopted in the Zhengzhou Olympic Stadium of China as shown in figure 15. The radial and circular cables are the main load-bearing components, which greatly reduce the role of the main structure and effectively make the structure simple and lightweight. Based on the previous factory calibration tests, the developed EM sensor monitoring system was applied to measure cable tension in the Zhengzhou Olympic Stadium. The system provided a pulse excitation signal to the primary coil to magnetize the steel cable and obtained the analog signal from the sensing coil. After passing through a signal

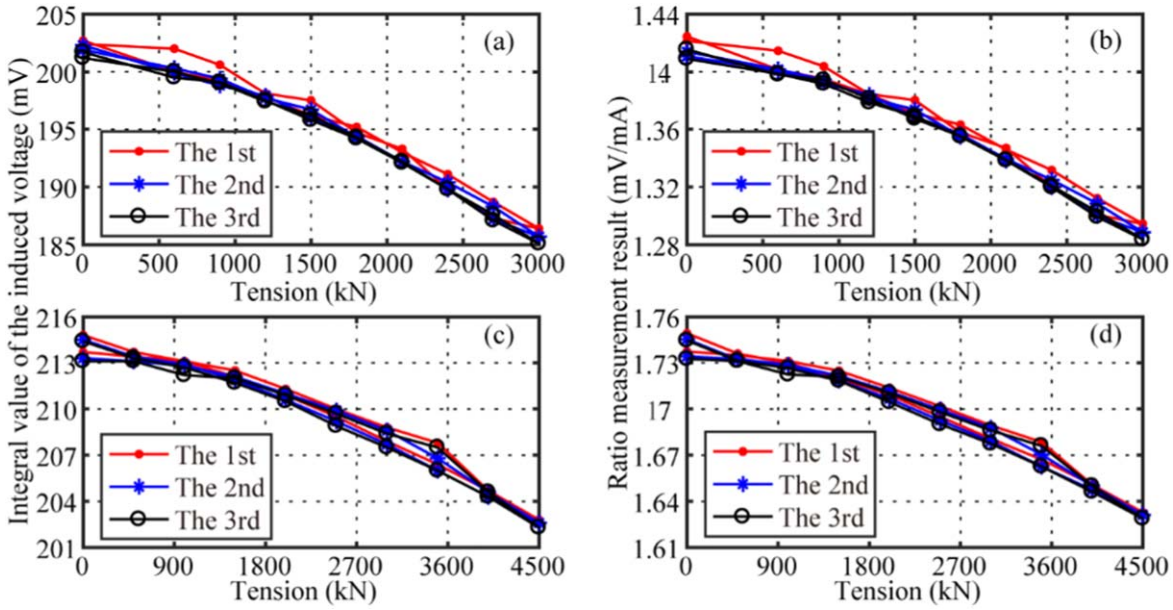

Figure 13. Three experimental results of two measurement methods ((a) integral value of the induced voltage results of radial cable (b) ratio measurement results of radial cable (c) integral value of the induced voltage results of circular cable (d) ratio measurement results of circular cable).

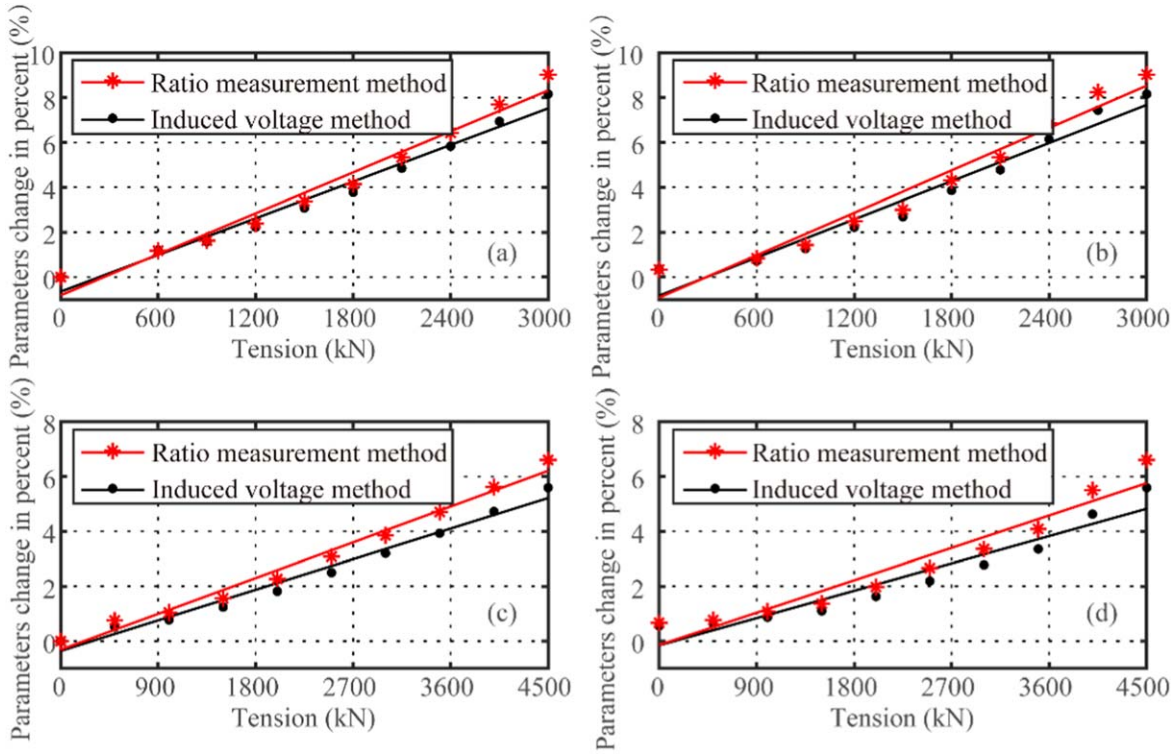

Figure 14 The relative sensitivity variations of the two measurement methods in radial cable during (a) loading and (b) unloading processes and in circular cable during (c) loading and (d) unloading processes.

Table 3. Comparison of relative sensitivity in two measurement methods.

	Ratio measurement method		Induced voltage method	
Relative sensitivity (%/kN)	Loading	Unloading	Loading	Unloading
Radial cable	0.3	0.31	0.27	0.28
Circular cable	0.14	0.13	0.12	0.11

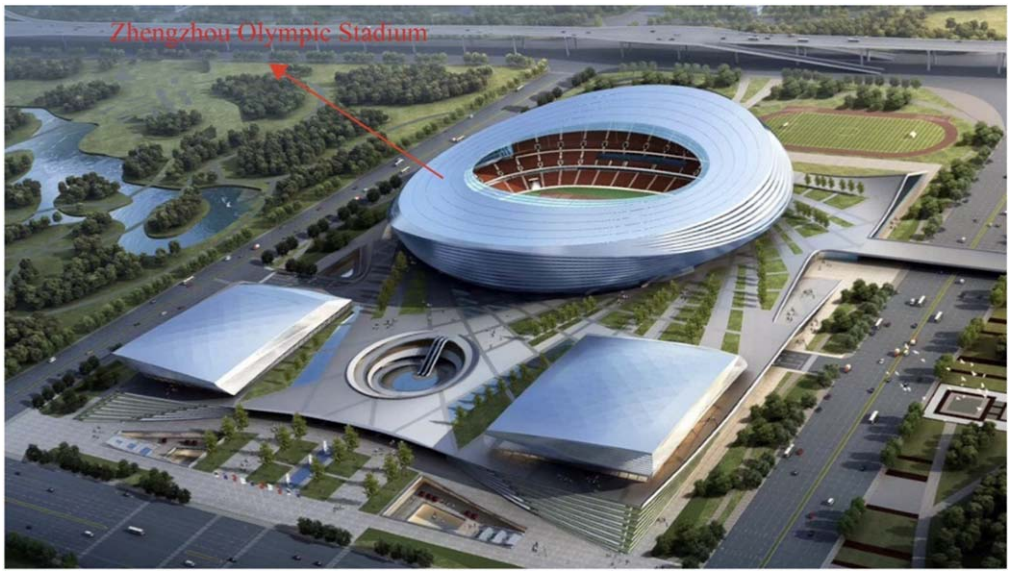

Figure 15. Zhengzhou Olympic Stadium.

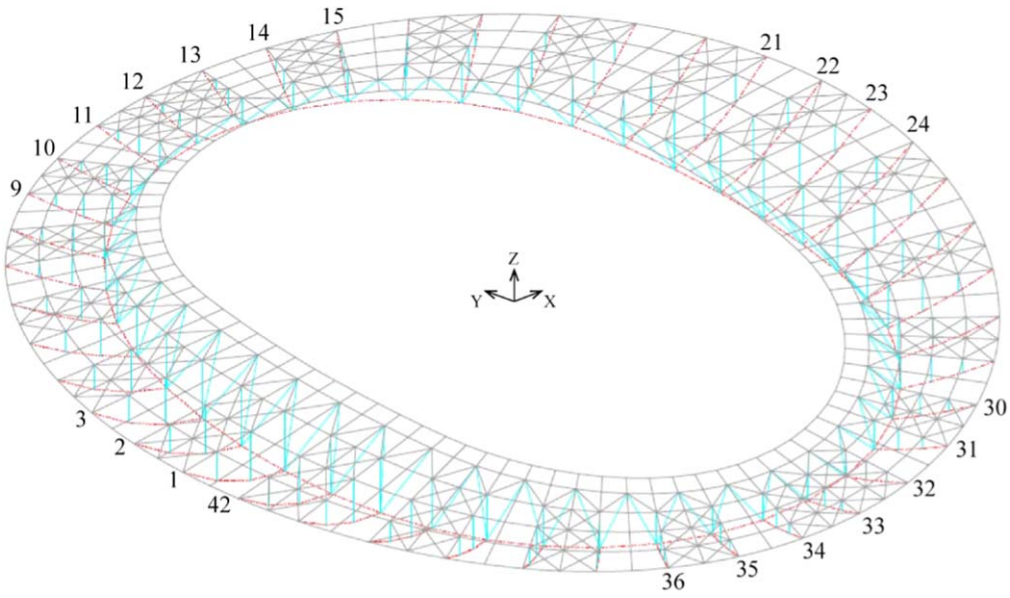

Figure 16. Numbering of the radial cables with the EM sensor installation.

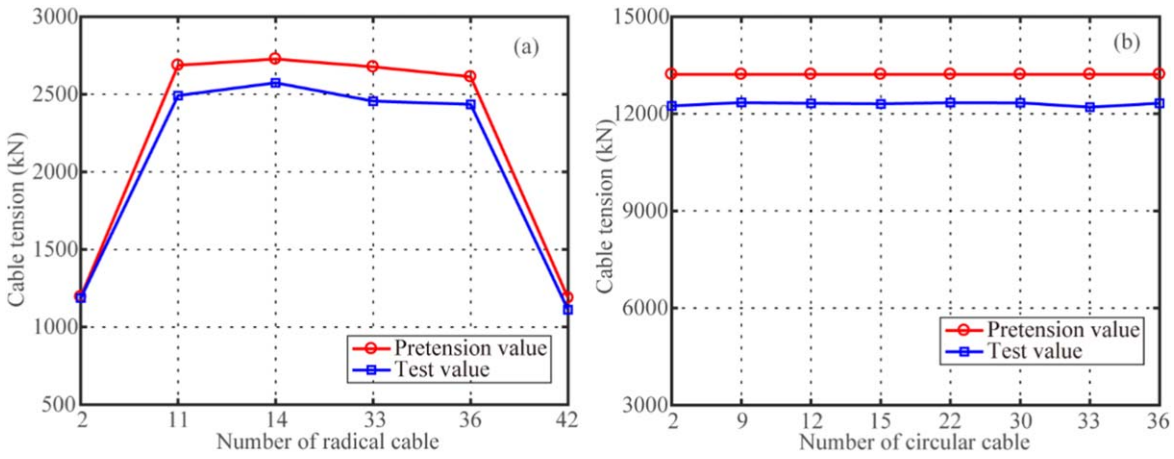

Figure 17. Measurement results of the (a) radial and (b) circular cables.

Figure 18. Photograph of EM sensor during the construction.

Table 4. Measurement data of radial cable for four days.

Ratio coefficient	Initial data	Temperature coefficient	Initial temperature (°C)	Date	Measurement data	Temperature (°C)	Tension (kN)
−22 589	1.4168	−0.008	23.94	28/03	1.4085	22.1	520
					1.4024	22.7	549
					1.3953	23.43	578
					1.3909	24.04	567
					1.3859	24.79	544
					1.3783	25.67	557
				01/04	1.3240	31.3	766
					1.3203	31.86	749
					1.3206	32.35	653
					1.3159	32.77	684
					1.3135	33.25	651
					1.3064	33.72	727
				04/04	1.3834	21.35	1223
					1.3741	22.5	1225
					1.3690	23.39	1179
					1.3589	24.74	1163
					1.3512	25.55	1189
					1.3406	26.82	1199
				10/04	1.3860	21.45	1146
					1.3765	21.86	1286
					1.3770	22.18	1217
					1.3739	22.9	1157
					1.3719	23.44	1105
					1.3658	23.94	1152

processing device and an A/D conversion circuit, the input and output signals were automatically acquired by the LabVIEW monitoring module to calculate the cable tension. The numbering of the radial cables installed with the EM sensor is shown in figure 16.

The radial cables were pulled to the pretension value using the hydraulic jack under stepwise loading below the yielding strength. Figured 17(a) and (b) show the measurement results of the radial and circular cables, which are plotted using the numbering of the radial cable as the abscissa and using the pretension and test values of the radial and circular cables as the ordinate. It is observed that the two sets of results between the pretension value and the test value are in good agreement, with relative errors less than 8.3% in the radial cables and 7.7% in the circular cables.

5.2. Tensioning process

Circular cable tension forces can be changed due to tensioning work on the radial cables of the stadium. Tension force variations were monitoring by EM sensors using the ratio measurement method. A temperature gauge was attached to each EM sensor to measure the ambient temperature. The sensor output signal would be influenced by variation of the coil resistance because of the temperature effect. Most studies have used the linear relationship between temperature and

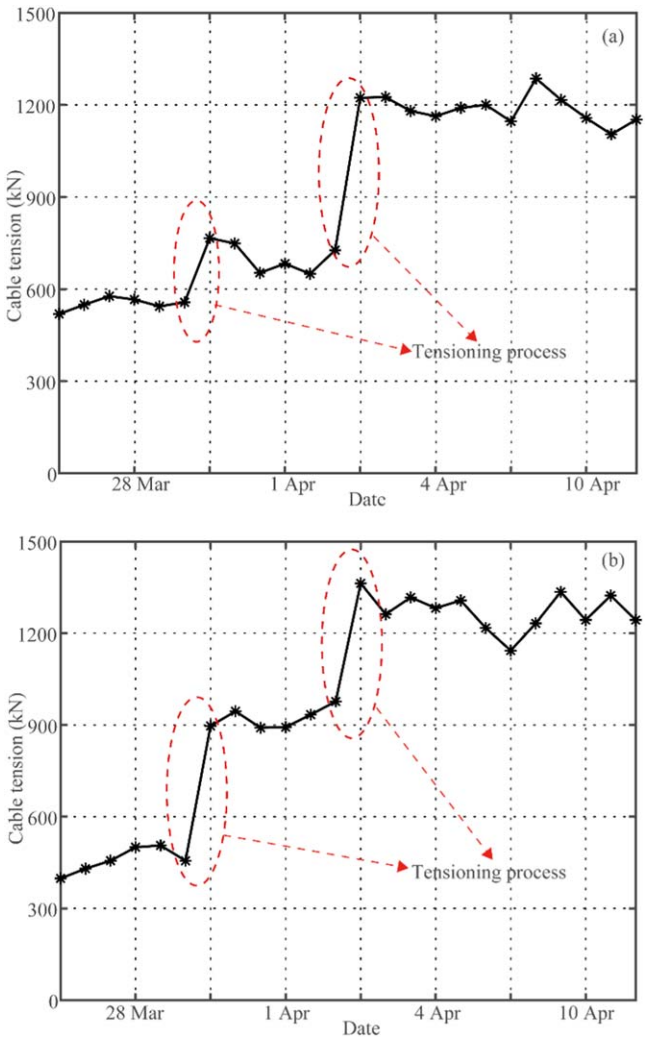

Figure 19. Test results for four days in (a) radial and (b) circular cables.

tension force, which can be taken into account in the calibration equation [35]. The tension-ratio ($F-R$) relationship equation can be written as:

$$F = F_0 + a((R - R_0) - b(T - T_0)), \tag{19}$$

where R_0 is the ratio result recorded at the known reference load F_0 and temperature T_0, T is the temperature, $a = dF/dR$ is the force to ratio result slope at the reference temperature T_0 and $b = dR/dT$ is the ratio result to temperature sensitivity.

According to the equation (19), the effect of temperature on the sensor was removed, while the effect of temperature on the structure still existed, a result that will be studied in future works. In the tensioning process, the steel cables were pulled by the hydraulic jack up to the design tension, which was completed on 4 April, 2018. The actual applied figure was shown in figure 18 and relevant measurement data were listed in the table 4. Figure 19 shows the test results for four days before and after the tensioning processes. The monitoring data is helpful for assessing the health status of the Zhengzhou Olympic Stadium.

It can be seen in figure 19 that the radial and circular cables showed large tension changes due to the tensioning work on 1 and 4 April, respectively. As the first and second tensioning works, the tension of the radial and circular cables reaches to the design value and remains almost unchanged after the tensioning work is completed, suggesting that the EM sensor using the ratio measurement method can sensitively detect variations in cable tension.

6. Conclusions and future works

The paper presented the EM sensor for monitoring cable tension using an innovative ratio measurement method. The LR model of the excitation system was proposed to illustrate that difference in the device channel or variation of the external wire resistance influences the excitation current, resulting in an inaccurate induced voltage variation in the secondary coil of the EM sensor. Furthermore, the transformer model of the sensor system was established to obtain the explicit relationship between the ratio result and the external tension. The ratio result of the integral value of the induced voltage to the excitation current variation was defined as the parameter proportional to relative permeability in the cable tension measurement. From observation of the experimental results of the factory calibration, it is confirmed that the ratio results increase almost linearly as the external tension increases. This result demonstrates a linear relationship between the ratio result and the external tension, a finding that agrees well with the theoretical derivation. Moreover, the simulation analysis and experiment result demonstrate that the ratio measurement method improves sensor performance with the comparison of the traditional induced voltage method. Utilization of the ratio measurement method improves the relative sensitivity of the sensor by 11.1% from 0.27%/kN to 0.3%/kN and by 10.7% from 0.28%/kN to 0.31%/kN in factory calibration of the radial cable in the loading and unloading processes, respectively. Future works will make a comparison between the force transducers and the EM sensors and involve the design of a split coil that can replace the traditional skeleton coil to facilitate installation of the sensor in engineering practice.

Acknowledgments

This work was supported by the Science Fund for Creative Research Groups of the National Natural Science Foundation of China (No. 51421064), the National Key Basic Research and Development Program (973 Program) (No. 2015CB060000), the scholarship under the State Scholarship Fund (No. 201706060109) and the Fundamental Research Funds for the Central Universities (DUT15YQ107). These grants are greatly appreciated.

ORCID iDs

Chengzhu Xiu https://orcid.org/0000-0002-4059-2990
Ye Lu https://orcid.org/0000-0002-2319-7681

References

[1] Yi T H and Li H N 2012 Methodology developments in sensor placement for health monitoring of civil infrastructures *Int. J. Distrib. Sens. Netw.* **8** 612726

[2] Li H N, Li D S, Ren L, Yi T H, Jia Z G and Li K P 2016 Structural health monitoring of innovative civil engineering structures in Mainland China *Struct. Monit. Maint.* **3** 1–32

[3] Chae M J, Yoo H S, Kim J Y and Cho M Y 2012 Development of a wireless sensor network system for suspension bridge health monitoring *Autom. Constr.* **21** 237–52

[4] Sim S H, Li J, Jo H, Park J W, Cho S, Spencer B F Jr and Jung H J 2014 A wireless smart sensor network for automated monitoring of cable tension *Smart Mater. Struct.* **23** 025006

[5] Duan Y F, Zhang R, Zhao Y, Or S W, Fan K Q and Tang Z F 2011 Smart elasto-magneto-electric (EME) sensors for stress monitoring of steel structures in railway infrastructures *J. Zhejiang Univ.-Sci.* A **12** 895–901

[6] Maruccio C, Quaranta G, Lorenzis L D and Monti G 2016 Energy harvesting from electrospun piezoelectric nanofibers for structural health monitoring of a cable-stayed bridge *Smart Mater. Struct.* **25** 085040

[7] Martínez-Castro R E, Jang S, Nicholas J and Bansal R 2017 Experimental assessment of an RFID-based crack sensor for steel structures *Smart Mater. Struct.* **26** 085035

[8] Xiu C Z, Ren L, Li H N and Jia Z G 2017 Study on an innovative self-inductance tension eddy current sensor based on the inverse magnetostrictive effect *Sens. Rev.* **37** 43–53

[9] Cho S J, Yim J, Shin S W, Jung H J, Yun C B and Wang M L 2013 Comparative field study of cable tension measurement for a cable-stayed bridge *J. Bridge Eng.* **18** 748–57

[10] Cho S, Lynch J P, Lee J J and Yun C B 2009 Development of an automated wireless tension force estimation system for cable-stayed bridges *J. Intell. Mater. Syst. Struct.* **21** 361–76

[11] Li H, Zhang F J and Jin Y Z 2014 Real-time identification of time-varying tension in stay cables by monitoring cable transversal acceleration *Struct. Control Health Monit.* **21** 1100–17

[12] Heo G and Joonryong J 2014 Semi-active vibration control in cable-stayed bridges under the condition of random wind load *Smart Mater. Struct.* **23** 075027

[13] Bao Y Q, Shi Z Q, Beck J L, Li H and Hou T Y 2017 Identification of time-varying cable tension forces based on adaptive sparse time-frequency analysis of cable vibrations *Struct. Control Health Monit.* **24** e1889

[14] Wu W H, Chen C C, Chen Y C, Lai G and Huang C M 2018 Tension determination for suspenders of arch bridge based on multiple vibration measurements concentrated at one end *Measurement* **123** 254–69

[15] Duan Y F, Zhang R, Dong C Z, Luo Y Z, Or S W, Zhao Y and Fan K Q 2016 Development of elasto-magneto-electric (EME) sensor for in-service cable force monitoring *Int. J. Struct. Stab. Dyn.* **16** 1640016

[16] Li H N, Xiu C Z and Ren L 2017 Influence of bias magnetic field for sleeve eddy current sensor (SECS) in tension measurement *Sensors Actuators* A **263** 451–60

[17] Zhang R, Duan Y F, Or S W and Zhao Y 2014 Smart elasto-magneto-electric (EME) sensors for stress monitoring of steel cables: design theory and experimental validation *Sensors* **14** 13644–60

[18] Xiu C Z, Ren L and Li H N 2017 Investigation on eddy current sensor in tension measurement at a resonant frequency *Appl. Sci.* **7** 538

[19] Singh V, Wang M L and Lloyd G M 2005 Measuring and modeling of corrosion in structural steels using magnetoelastic sensors *Smart Mater. Struct.* **14** S24–31

[20] Sumitro S and Wang M L 2005 Sustainable structural health monitoring system *Struct. Control Health Monit.* **12** 445–67

[21] Kim J, Kim J W, Lee C and Park S 2017 Development of embedded em sensors for estimating tensile forces of PSC girder bridges *Sensors* **17** s17091989

[22] Liu X C, Wu D H, He C F, Feng H and Wu B 2018 Comparison of AC and pulsed magnetization-based elasto-magnetic methods for tensile force measurement in steel strand *Measurement* **117** 410–8

[23] Ricken W, Liu J G and Becker W J 2001 GMR and eddy current sensor in use of stress measurement *Sensors Actuators* A **91** 42–5

[24] Ricken W, Schoenekess H C and Becker W J 2006 Improved multi-sensor for force measurement of pre-stressed steel cables by means of the eddy current technique *Sensors Actuators* A **129** 80–5

[25] Schoenekess H C, Ricken W and Becker W J 2007 Method to determine tensile stress alterations in prestressing steel strands by means of an eddy-current technique *IEEE. Sens. J.* **7** 1200–5

[26] Roy D, Kumar Kaushik B and Chakraborty R 2013 A novel E-shaped coil for eddy current testing *Sens. Rev.* **33** 363–70

[27] Tang D D, Huang S J, Chen W M and Jiang J S 2008 Study of a steel strand tension sensor with difference single bypass excitation structure based on the magneto-elastic effect *Smart Mater. Struct.* **17** 025019

[28] Tse P W, Liu X C, Liu Z H, Wu B, He C F and Wang X J 2011 An innovative design for using flexible printed coils for magnetostrictive-based longitudinal guided wave sensors in steel strand inspection *Smart Mater. Struct.* **20** 055001

[29] Cappello C, Zonta D, Laasri H A L, Glisic B and Wang M L 2018 Calibration of elasto-magnetic sensors on in-service cable-stayed bridges for stress monitoring *Sensors* **18** S18020466

[30] Sumitro S, Kurokawa S J, Shimano K J and Wang M L 2005 Monitoring based maintenance utilizing actual stress sensory technology *Smart Mater. Struct.* **14** S68–78

[31] Zhou D Q, Wang J, He Y Z, Chen D W and Li K 2016 Influence of metallic shields on pulsed eddy current sensor for ferromagnetic materials defect detection *Sensors Actuators* A **248** 162–72

[32] Adewale I D and Tian G Y 2013 Decoupling the influence of permeability and conductivity in pulsed eddy-current measurements *IEEE Trans. Magn.* **49** 1119–27

[33] Tian G Y, He Y Z, Adewale I and Simm A 2013 Research on spectral response of pulsed eddy current and NDE applications *Sensors Actuators* A **189** 313–20

[34] Tian G Y, Li Y and Mandache C 2009 Study of Lift-Off invariance for pulsed eddy-current signals *IEEE Trans. Magn.* **45** 184–91

[35] Yim J, Wang M L, Shin S W, Yun C B, Jung H J, Kim J T and Eem S H 2013 Field application of elasto-magnetic stress sensors for monitoring of cable tension force in cable-stayed bridges *Smart Struct. Syst.* **12** 465–82